Title
Relationship between Mobility and Lattice Strain in Electrochemically Doped Poly(3-hexylthiophene)

Journal
ACS Macro Letters, 4(12)

Authors
Thelen, JL
Wu, SL
Javier, AE
et al.

Publication Date
2015-11-25

DOI
10.1021/acsmacrolett.5b00827

Peer reviewed

ACS Macro Letters

Letter

pubs.acs.org/macroletters

Relationship between Mobility and Lattice Strain in Electrochemically Doped Poly(3-hexylthiophene)

Jacob L. Thelen,[†,‡,§] Shao-Ling Wu,[§,∥] Anna E. Javier,[§,∥] Venkat Srinivasan,[§,∥] Nitash P. Balsara,[†,‡,§,∥] and Shrayesh N. Patel*[,†,‡,∥,⊥]

[†]Department of Chemical and Biomolecular Engineering, University of California, Berkeley, California 94720, United States
[‡]Materials Sciences Division, [§]Joint Center for Energy Storage Research (JCESR), and [∥]Environmental Energy Technologies Division, Lawrence Berkeley National Laboratory, Berkeley, California 94720, United States

Supporting Information

ABSTRACT: Conjugated semiconducting polymers, such as poly(3-hexylthiophene) (P3HT), are poised to play an integral role in the development of organic electronic devices; however, their performance is governed by factors that are intrinsically coupled: dopant concentration, carrier mobility, crystal structure, and mesoscale morphology. We utilize synchrotron X-ray scattering and electrochemical impedance spectroscopy to probe the crystal structure and electronic properties of P3HT *in situ* during electrochemical doping. We show that doping strains the crystalline domains, coincident with an exponential increase in hole mobility. We believe these observations provide guidance for the development of improved theoretical models for charge transport in semiconducting polymers.

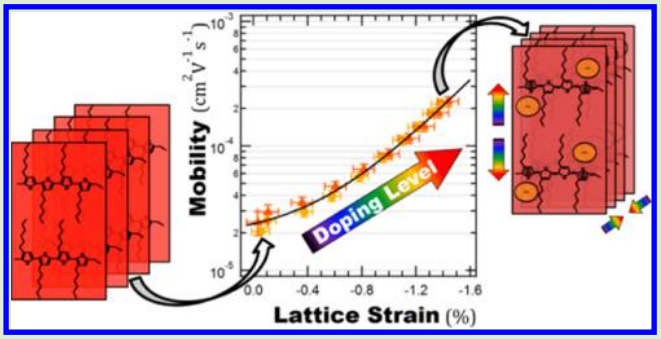

The mechanism of charge transport within conjugated semiconducting polymers has been the subject of extensive study for decades, especially in recent years with the advent of commercial applications such as organic photovoltaics (OPVs), organic field effect transistors (OFETs), and organic light-emitting diodes (OLEDs).[1−3] A common feature of all semiconducting polymers is a high degree of structural disorder, which generally requires an intermolecular hopping mechanism to achieve macroscopic charge transport.[4,5] While models that describe electron transport in completely disordered semiconducting polymers have been developed,[6,7] the performance of many materials, such as poly(3-hexylthiophene) (P3HT), are complicated by their semicrystalline nature, which creates discrete regions of higher structural order within a disordered amorphous matrix.[8−11] The electronic performance of these materials has been shown to be significantly influenced by the degree of ordering, which in turn can be affected by polymer molecular weight, purity, and processing conditions.[12−15] In addition to all of these complexities, the method of producing charge carriers (e.g., field effect, chemical doping, or electrochemical doping) and their total concentration can lead to measured carrier mobilities that differ by up to 4 orders of magnitude.[12,16−18] Establishing the underpinnings of experimental observations is nontrivial due to these competing and interrelated effects. The goal of this work is to present clear experimental evidence of how doping influences the microstructure and electronic properties of P3HT while all other parameters that affect charge transport are kept constant.

The key to our experimental approach is the use of the block copolymer poly(3-hexylthiophene)-*b*-poly(ethylene oxide) (P3HT-PEO). P3HT-PEO has previously been shown to microphase separate into nanoscale domains of P3HT-rich and PEO-rich phases. Previous studies have shown that the crystalline lattice of P3HT is not perturbed by the presence of the PEO block.[19,20] By adding an ionic species, such as lithium bis(trifluoromethanesulfonyl)imide (LiTFSI), the PEO-rich domains can act as an electrolyte, providing efficient transport of ionic species throughout the bulk material.[19,20] The intimate mixing of electrolyte and P3HT (i.e., each P3HT nanodomain is effectively a thin film surrounded by PEO/LiTFSI electrolyte) enables the construction of the solid-state electrochemical cell shown in Figure 1. The all-solid cell prevents any complexities that might arise from solvent swelling of the P3HT, thus any changes to the structure of P3HT during electrochemical doping can be directly attributed to the doping process itself. Furthermore, unlike most electrochemical doping studies, which utilize an electrode coated with a thin film of conjugated polymer soaked in an electrolyte, the P3HT-PEO/LiTFSI layer in our solid-state cell is typically ∼350 μm thick. The thick film geometry allows us to effectively measure the bulk electronic properties (through-plane) and the bulk P3HT microstructure (transmission geometry) *in situ* during electrochemical doping. To our knowledge, this is the first time that

Received: November 17, 2015
Accepted: November 23, 2015
Published: November 25, 2015

DOI: 10.1021/acsmacrolett.5b00827
ACS Macro Lett. 2015, 4, 1386−1391

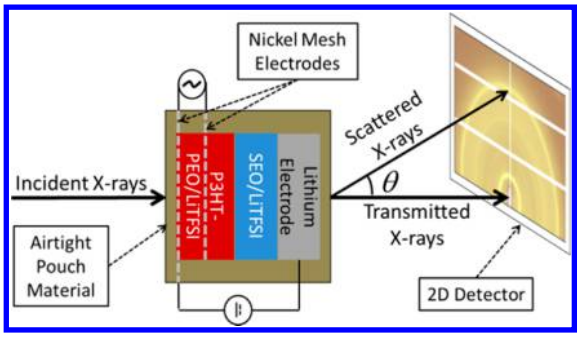

Figure 1. Schematic of the *in situ* electrochemical cell and the configuration used for WAXS measurements.

both the P3HT microstructure and its electronic properties have been simultaneously measured as a function of doping level.

The block copolymer studied in this work was synthesized, purified, and characterized using the techniques described by Javier et al.[19] It has a P3HT molecular weight (M_{P3HT}) of 7 kg mol^{-1} and a PEO molecular weight (M_{PEO}) of 2 kg mol^{-1} and will be referred to as P3HT-PEO(7−2). Salt-containing P3HT-PEO samples were prepared by mixing solutions of polymer (P3HT-PEO in benzene) and salt (LiTFSI in tetrahydrofuran), followed by freeze-drying to yield a solid powder of P3HT-PEO(7−2)/LiTFSI with a salt concentration of r = 0.085, where r denotes the molar ratio of Li^+ ions to ethylene oxide (EO) moieties.[20] The degree of P3HT crystallinity in the freeze-dried samples was determined to be 62% by differential scanning calorimetry using an ideal melting enthalpy of 33 J g^{-1} (see Supporting Information (SI) Section S1 for details).[21] Small-angle X-ray scattering (SAXS) was used to probe the nanostructure of P3HT-PEO(7−2)/LiTFSI, which was found to be consistent with the nanofibrillar morphology observed in previous work (SI Section S2).[19,20,22]

In situ electrochemical cells used for X-ray scattering were assembled using similar techniques to Patel et al.[22] (detailed description in SI Section S3). In short, the P3HT-PEO(7−2)/LiTFSI is contained within a spacer of defined area and thickness, with one nickel mesh electrode on the surface and another embedded within. A solid polymer electrolyte consisting of polystyrene-*b*-poly(ethylene oxide) (SEO) mixed with LiTFSI served as a separator, and lithium metal was used as the counter electrode. The entire cell was assembled and vacuum-sealed in an airtight pouch within an argon glovebox. A schematic of the sample cell is shown in Figure 1.

All experiments were performed at 90 °C to ensure that the PEO phase was amorphous with suitable ionic conductivity.[20] Electrochemical oxidation (doping) was performed galvanostatically between the outer nickel mesh electrode and the lithium electrode (anode) with a current density such that each oxidation step was completed in 30 min. Doping was performed in increments of r_{ox} = 0.005 or r_{ox} = 0.01, where r_{ox} is the ratio of electrons removed to the total number of hexylthiophene (HT) monomers. At the end of each oxidation step, the cell was allowed to relax for 20 min, and then the negative lead was disconnected from the lithium electrode and connected to the inner (embedded) nickel mesh electrode (see Figure 1). The conductive properties of the P3HT were then probed using potentiostatic electrochemical impedance spectroscopy (PEIS) between the two nickel mesh electrodes. The

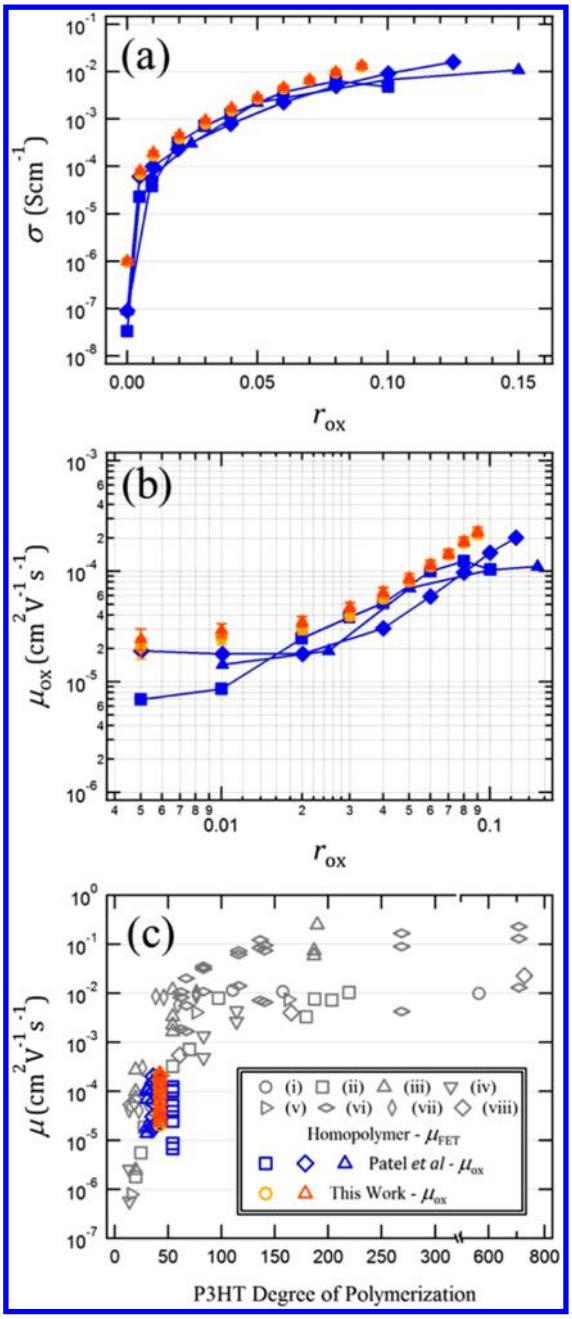

Figure 2. (a) Electronic conductivity plotted as a function of doping level for P3HT-PEO. Blue data are taken from ref 22: squares P3HT-PEO(9−2), diamonds P3HT-PEO(6−2), triangles P3HT-PEO(5−4). The yellow circles and orange triangles were measured for replicate samples of P3HT-PEO(7−2) in this work. (b) The corresponding mobility values from plot (a) as a function of doping level. (c) P3HT mobility plotted as a function of P3HT degree of polymerization for the P3HT-PEO samples [same data labels as (a) and (b)], along with the compilation of field effect mobility values (gray symbols) assembled by Noriega and Rivnay et al.[25] References to the individual studies are as follows: circles (i),[25] squares (ii),[26] triangles (iii),[27] upside-down triangles (iv),[28] sideways triangles (v),[13] horizontal diamonds (vi),[29] vertical diamonds (vii),[30] and square diamonds (viii).[31]

open-circuit potential between the two mesh electrodes was zero (within instrumental resolution) prior to commencing the impedance measurements, which implies a uniform charge distribution through the P3HT-PEO electrode. The bulk

DOI: 10.1021/acsmacrolett.5b00827
ACS Macro Lett. 2015, 4, 1386−1391

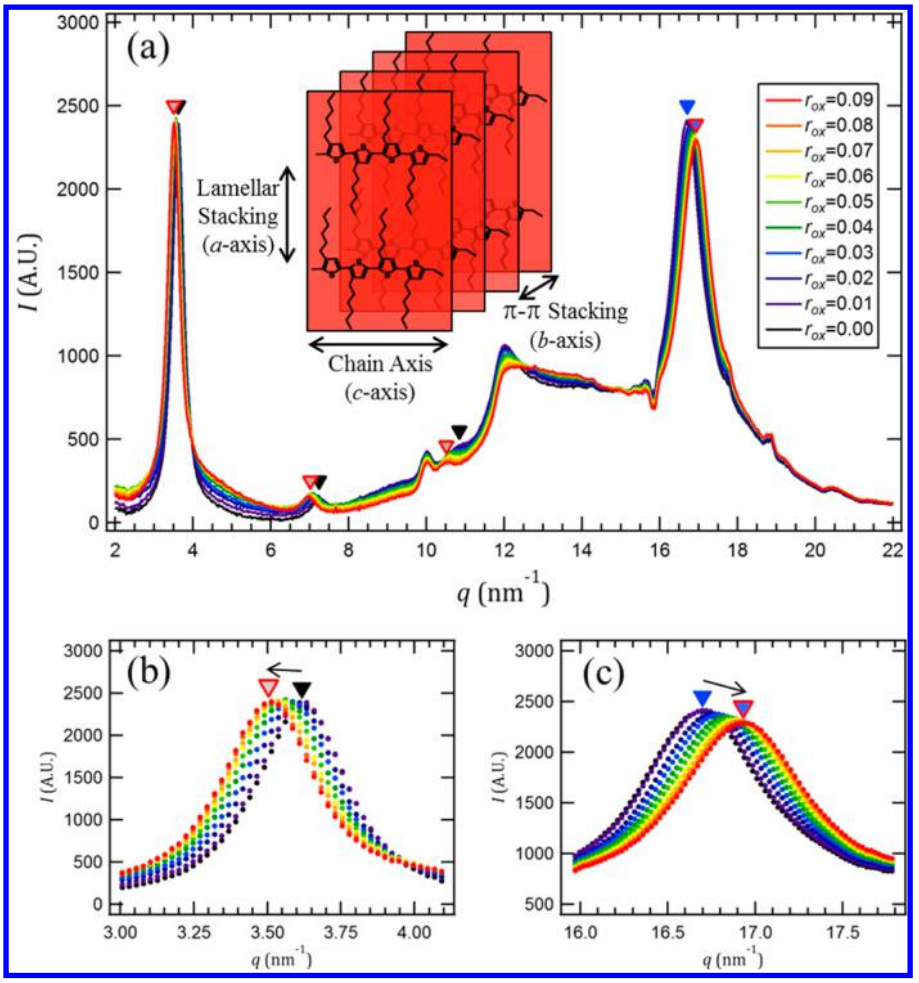

Figure 3. (a) Representative 1D WAXS profiles for one of the P3HT-PEO replicates for a range of doping levels. Peaks corresponding to P3HT (100, 200, 300, and 020) are indicated with triangle markers. The solid black and blue markers indicate the peak positions before doping, and the red highlighted markers indicate the peak positions at r_{ox} = 0.09. The inset provides a schematic for the crystal structure of P3HT. (b) Expanded view of the (100) peaks. (c) Expanded view of the (020) peaks.

conductivity of P3HT (σ) was calculated from $\sigma = \delta L/AR$, where δ is a correction factor to account for the mesh electrode geometry; L is the distance between the two nickel mesh electrodes; A is the area defined by the sample spacer; and R is the measured bulk electronic resistance. As noted previously,[22] there is hysteresis in the polymer properties between consecutive doping and dedoping experiments; all data shown in this letter are from the second oxidation cycle of both samples. Sections S4−S6 in the SI provide detailed information for the electrochemical oxidation and PEIS measurements, electrode geometry correction factor, and first (break-in) cycle conductivity values, respectively.

Two of such cells described above were taken to a synchrotron wide-angle X-ray scattering (WAXS) apparatus on Beamline 7.3.3 at the Advanced Light Source, Lawrence Berkeley National Laboratory.[23] The P3HT crystalline structure was probed *in situ* during electrochemical oxidation by performing WAXS measurements immediately after PEIS measurements, approximately 30 min after each oxidation step. The isotropic 2D scattering patterns were azimuthally integrated using the Nika macro developed by Jan Ilavsky[24] to yield 1D data sets of intensity (I) versus the magnitude of the scattering vector, $q = (4\pi/\lambda)\sin(\theta/2)$, where λ is the radiation wavelength and θ is the scattering angle depicted in Figure 1. Scattering intensity from a sample cell containing all of the components except the P3HT-PEO(7−2)/LiTFSI was used for background correction (SI Section S7). Peak positions of interest (q^*) were determined by fitting the corrected WAXS data in the vicinity of the peak with a Lorentzian function of the form, $I(q) = I_0 + C_1/((q - q^*)^2 + C_2)$, where I_0, C_1, C_2, and q^* were varied in Igor Pro's built-in Levenberg−Marquardt nonlinear least-squares algorithm to achieve the best fit.

In Figure 2a, we plot P3HT conductivity as a function of doping level from two replicate samples. The data are consistent with those obtained previously for electrochemically doped P3HT-PEO,[22] which were corrected by the electrode geometry factor (δ) (see SI Section S5) and are plotted for comparison. The increase in conductivity seen in Figure 2a can, in principle, be attributed to changes in both carrier concentration and carrier mobility. We calculate mobility (μ_{ox}) using $\mu_{ox} = \sigma/ne$, where n is the electrochemically generated charge carrier density and e the elementary charge.[22] We assume all current transferred between the electrodes of the electrochemical cell goes directly toward generating charge carriers. Consequently, n is the upper limit for charge carrier density, which in turn yields the lower bound for the calculated charge carrier mobility. In Figure 2b, we plot mobility as a function of doping level. It is clear from Figure 2b that the level of electrochemical doping in P3HT-PEO(7−2)/LiTFSI strongly influences carrier mobility.

DOI: 10.1021/acsmacrolett.5b00827
ACS Macro Lett. 2015, 4, 1386−1391

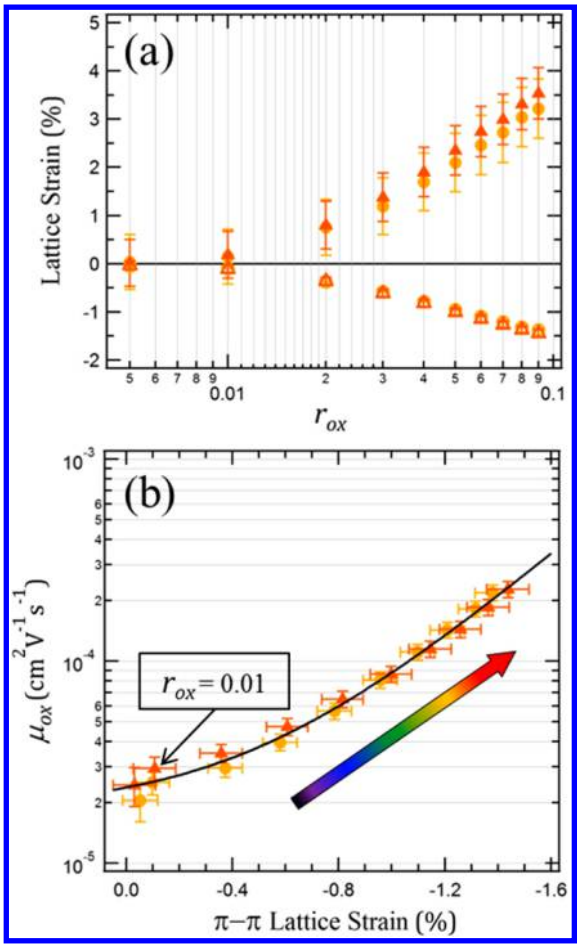

Figure 4. (a) Lattice strain of the two replicate samples plotted as a function of doping level. Closed symbols correspond to the lamellar stacking (100) spacing, and open symbols represent the $\pi-\pi$ stacking (020) spacing. (b) Mobility plotted as a function of the $\pi-\pi$ lattice strain for the two replicate samples in this work. The solid line represents the best fit of $\mu_{ox} = y_0 + De^{(-\tau\alpha)}$, where α is the $\pi-\pi$ lattice strain (%) and y_0, D, and τ are fit parameters found to be $y_0 = 1.8(3) \times 10^{-5}$ (cm^2 V^{-1} s^{-1}), $D = 5(1) \times 10^{-6}$ (cm^2 V^{-1} s^{-1}), and $\tau = 2.6(2)$. The colored arrow indicates the direction of increasing doping level.

For reference, in Figure 2c we plot the hole mobility of P3HT measured by electrochemical doping of P3HT-PEO/LiTFSI with the comprehensive list of homopolymer P3HT field effect mobility values (μ_{FET}) formerly assembled by Noriega and Rivnay et al.[8] The abscissa in Figure 2c is the average degree of polymerization of P3HT. Agreement is seen between the two approaches for $r_{ox} \geq 0.06$ despite the differences in polymer samples (block copolymer versus homopolymer), doping mechanisms, and direction of measurement (in-plane versus through-plane). Similar observations for P3HT homopolymer soaked in liquid electrolytes have been reported,[17] suggesting that the P3HT domains in P3HT-PEO conduct through the same mechanism as homopolymer P3HT.

The impact of electrochemical doping on the P3HT microstructure is revealed through the WAXS profiles shown in Figure 3. Scattering peaks corresponding to the (h00) direction are observed at 3.62 nm^{-1} (100), 7.23 nm^{-1} (200), and 10.9 nm^{-1} (300) in the undoped polymer ($r_{ox} = 0$). These peaks correspond to the lamellar stacking of the P3HT backbones and are labeled with black triangles. The peak observed at 16.7 nm^{-1} in the undoped polymer ($r_{ox} = 0$), labeled by a blue triangle, corresponds to the (020) direction and is related to the $\pi-\pi$ stacking distance between adjacent chains.[32−35] A schematic of the P3HT structure is provided in the inset of Figure 3a. Any unlabeled peak in Figure 3a can be attributed to the parasitic scattering from the electrochemical cell (Figure S7 in the SI). All of the WAXS peaks related to the P3HT crystal structure shift upon doping. The lamellar stacking peaks shift to lower q-values (Figure 3b), while the $\pi-\pi$ stacking peak shifts to higher q-values (Figure 3c) as P3HT is oxidized. The oxidation of P3HT is balanced by the deposition of lithium on the anode (see Figure 1). The TFSI$^-$ anion left behind in the process must migrate into the P3HT microphase to balance the charge from the hole generated by the removal of an electron from P3HT. The expansion of the lamellar stacking seen in Figure 3b is attributed to the incorporation of the TFSI$^-$ anions into the lattice. This result is consistent with the results of Kawai and co-workers, where homopolymer P3HT films were electrochemically doped in an electrolyte bath,[36,37] as well as the analogous intercalation of small molecules and fullerenes between the side chains of other conjugated polymer systems.[38] Interestingly, electrochemical doping results in a contraction of the $\pi-\pi$ stacking distance (Figure 3c). Although the exact nature of the stress that induces the $\pi-\pi$ stacking contraction is still under investigation, we demonstrate below that the decrease in the distance between polymer chains in the $\pi-\pi$ stacking direction is strongly correlated with the observed increase in hole mobility as the doping level is increased. It is important to note that the widths and areas under each peak are unaffected by doping, indicating that crystallinity is not disrupted by the intercalation of the TFSI$^-$ dopant ion. Furthermore, no additional scattering peaks are observed as doping is increased; therefore, we conclude that all of the observed structural changes can simply be viewed as doping-induced strains to the existing orthorhombic crystal lattice of undoped P3HT.[33,36,37,39]

We quantify the lattice strain in the P3HT crystal structure by lattice strain (%) = $((d(r_{ox}) - d_0)/d_0) \times 100$, where $d(r_{ox})$ and d_0 are the doped and undoped real-space lattice dimensions, respectively, determined from either the (100) lamellar stacking or the (020) $\pi-\pi$ stacking peak positions. Figure 4a quantifies the effect of electrochemical oxidation on the P3HT lattice in the lamellar and $\pi-\pi$ stacking directions. Comparing Figures 2b and 4a reveals that both hole mobility and lattice strain scale with the logarithm of doping level for $r_{ox} > 0.01$. It is widely accepted that macroscopic transport in P3HT is limited by the rate of interchain hopping in the $\pi-\pi$ stacking direction, where there is the largest degree of interchain coupling.[4,40] In Figure 4b we plot the hole mobility as a function of the $\pi-\pi$ stacking lattice strain wherein a clear exponential relationship between the mobility and $\pi-\pi$ interchain spacing is observed. Interestingly, hopping-based models predict that mobility is proportional to the square of the interchain charge transfer integral (t^2), which is often modeled as an exponential, $t = t_0e^{(-\gamma a)}$, where a is the intersight ($\pi-\pi$ interchain) distance and the prefactor (t_0) and exponential coefficient (γ) govern the extent to which lattice structure influences charge transport.[4,25,41] Although other factors such as changes in the density of states (DOS) will also contribute to the observed changes in mobility with doping level,[5,6,42] the clear correlation between lattice strain and mobility demonstrates that structural changes during electrochemical doping are intrinsically linked to the subsequent charge transport characteristics of electrochemically doped conjugated polymers.

DOI: 10.1021/acsmacrolett.5b00827
ACS Macro Lett. 2015, 4, 1386−1391

In summary, through the use of a custom-designed all solid-state electrochemical cell, we have conclusively demonstrated that electrochemical doping of P3HT induces systematic changes to the packing structure of crystalline P3HT domains. The induced strains in the crystalline lattice, positive in the (100) direction and negative in the (020) direction, facilitate the incorporation of anionic ($TFSI^-$) dopants and tighter packing in the $\pi-\pi$ stacking direction. *In situ* measurement of the conductive properties of the P3HT, which allowed us to directly compare the mobility of hole charge carriers with the induced strains in the P3HT lattice, revealed an exponential relationship between the $\pi-\pi$ stacking distance and the measured mobility. We believe that our results shed new light on the interplay between crystal structure, dopant concentration, and charge transport in semicrystalline conjugated polymers.

■ ASSOCIATED CONTENT

Supporting Information

The Supporting Information is available free of charge on the ACS Publications website at DOI: 10.1021/acsmacrolett.5b00827.

Detailed description of the % crystallinity analysis (S1); mesoscale structure analysis through SAXS (S2); solid-state sample preparation (S3); electrochemical oxidation and PEIS measurements (S4); mesh electrode geometry correction factor (δ) determination (S5); data from first electrochemical oxidation (break-in) cycle (S6); and WAXS background correction (S7) (PDF)

■ AUTHOR INFORMATION

Corresponding Author

*E-mail: shrayesh@berkeley.edu.

Present Address

[⊥]S.N.P.: Materials Research Laboratory, University of California, Santa Barbara, California 93106, United States.

Notes

The authors declare no competing financial interest.

■ ACKNOWLEDGMENTS

This work was primarily supported by the Joint Center for Energy Storage Research, an Energy Innovation Hub funded by the U.S. Department of Energy (DOE), Office of Science, Basic Energy Sciences (BES). X-ray scattering experiments were performed at Lawrence Berkeley National Laboratory's Advance Light Source, Beamline 7.3.3. Beamline 7.3.3 of the Advanced Light Source is supported by the Director of the Office of Science, Office of Basic Energy Sciences, of the U.S. Department of Energy under Contract No. DE-AC02-05CH11231.

■ REFERENCES

(1) Malliaras, G.; Friend, R. *Phys. Today* **2005**, *58*, 53−58.
(2) Berggren, M.; Nilsson, D.; Robinson, N. D. *Nat. Mater.* **2007**, *6*, 3−5.
(3) Facchetti, A. *Chem. Mater.* **2011**, *23*, 733−758.
(4) Coropceanu, V.; Cornil, J.; da Silva Filho, D. A.; Olivier, Y.; Silbey, R.; Brédas, J.-L. *Chem. Rev.* **2007**, *107*, 926−952.
(5) Laquai, F.; Wegner, G.; Bässler, H. *Philos. Trans. R. Soc., A* **2007**, *365*, 1473−1487.
(6) Coehoorn, R.; Pasveer, W. F.; Bobbert, P. A.; Michels, M. A. *J. Phys. Rev. B: Condens. Matter Mater. Phys.* **2005**, *72*, 155206.
(7) Noriega, R.; Salleo, A.; Spakowitz, A. *J. Proc. Natl. Acad. Sci. U. S. A.* **2013**, *110*, 16315−16320.
(8) Noriega, R.; Rivnay, J.; Vandewal, K.; Koch, F. P. V; Stingelin, N.; Smith, P.; Toney, M. F.; Salleo, A. *Nat. Mater.* **2013**, *12*, 1038−1044.
(9) Mollinger, S. a.; Krajina, B. a.; Noriega, R.; Salleo, A.; Spakowitz, A. *J. ACS Macro Lett.* **2015**, *4*, 708−712.
(10) Gao, J.; Niles, E. T.; Grey, J. K. *J. Phys. Chem. Lett.* **2013**, *4*, 2953−2957.
(11) Poelking, C.; Andrienko, D. *Macromolecules* **2013**, *46*, 8941.
(12) Jiang, X.; Harima, Y.; Yamashita, K.; Tada, Y.; Ohshita, J.; Kunai, A. *Chem. Phys. Lett.* **2002**, *364*, 616−620.
(13) Zen, A.; Saphiannikova, M.; Neher, D.; Grenzer, J.; Grigorian, S.; Pietsch, U.; Asawapirom, U.; Janietz, S.; Scherf, U.; Lieberwirth, I.; et al. *Macromolecules* **2006**, *39*, 2162−2171.
(14) Brinkmann, M. *J. Polym. Sci., Part B: Polym. Phys.* **2011**, *49*, 1218−1233.
(15) Duong, D. T.; Wang, C.; Antono, E.; Toney, M. F.; Salleo, *A. Org. Electron.* **2013**, *14*, 1330−1336.
(16) Harima, Y.; Eguchi, T.; Yamashita, K. *Synth. Met.* **1998**, *95*, 69−74.
(17) Shimotani, H.; Diguet, G.; Iwasa, Y. *Appl. Phys. Lett.* **2005**, *86*, 022104.
(18) Harima, Y.; Kunugi, Y.; Yamashita, K.; Shiotani, M. *Chem. Phys. Lett.* **2000**, *317*, 310−314.
(19) Javier, A. E.; Patel, S. N.; Hallinan, D. T.; Srinivasan, V.; Balsara, N. P. *Angew. Chem., Int. Ed.* **2011**, *50*, 9848−9851.
(20) Patel, S. N.; Javier, A. E.; Stone, G. M.; Mullin, S. A.; Balsara, N. P. *ACS Nano* **2012**, *6*, 1589−1600.
(21) Balko, J.; Lohwasser, R. H.; Sommer, M.; Thelakkat, M.; Thurn-Albrecht, T. *Macromolecules* **2013**, *46*, 9642−9651.
(22) Patel, S. N.; Javier, A. E.; Balsara, N. P. *ACS Nano* **2013**, *7*, 6056−6068.
(23) Hexemer, A.; Bras, W.; Glossinger, J.; Schaible, E.; Gann, E.; Kirian, R.; MacDowell, A.; Church, M.; Rude, B.; Padmore, H. *J. Phys. Conf. Ser.* **2010**, *247*, 012007.
(24) Ilavsky, J. *J. Appl. Crystallogr.* **2012**, *45*, 324−328.
(25) Noriega, R.; Rivnay, J.; Vandewal, K.; Koch, F. P. V; Stingelin, N.; Smith, P.; Toney, M. F.; Salleo, A. *Nat. Mater.* **2013**, *12*, 1038−1044.
(26) Kline, R. J.; McGehee, M. D.; Kadnikova, E. N.; Liu, J.; Fréchet, J. M. *J. Adv. Mater.* **2003**, *15*, 1519−1522.
(27) Kline, R. J.; McGehee, M. D.; Kadnikova, E. N.; Liu, J.; Fréchet, J. M. J.; Toney, M. F. *Macromolecules* **2005**, *38*, 3312−3319.
(28) Zen, a.; Pflaum, J.; Hirschmann, S.; Zhuang, W.; Jaiser, F.; Asawapirom, U.; Rabe, J. P.; Scherf, U.; Neher, D. *Adv. Funct. Mater.* **2004**, *14*, 757−764.
(29) Chang, J.-F.; Clark, J.; Zhao, N.; Sirringhaus, H.; Breiby, D.; Andreasen, J.; Nielsen, M.; Giles, M.; Heeney, M.; McCulloch, I. *Phys. Rev. B: Condens. Matter Mater. Phys.* **2006**, *74*, 115318.
(30) Zhang, R.; Li, B.; Iovu, M. C.; Jeffries-El, M.; Sauvé, G.; Cooper, J.; Jia, S.; Tristram-Nagle, S.; Smilgies, D. M.; Lambeth, D. N.; et al. *J. Am. Chem. Soc.* **2006**, *128*, 3480−3481.
(31) Verilhac, J.; Pokrop, R.; LeBlevennec, G.; Kulszewicz-Bajer, I.; Buga, K.; Zagorska, M.; Sadki, S.; Pron, A. *J. Phys. Chem. B* **2006**, *110*, 13305−13309.
(32) Prosa, T. J.; Winokur, M. J.; Moulton, J.; Smith, P.; Heeger, *A. J. Synth. Met.* **1993**, *55*, 370−377.
(33) Prosa, T.; Winokur, M.; Moulton, J.; Smith, P.; Heeger, A. *Phys. Rev. B: Condens. Matter Mater. Phys.* **1995**, *51*, 159−168.
(34) Winokur, M. J.; Wamsley, P.; Moulton, J.; Smith, P.; Heeger, A. *J. Macromolecules* **1991**, *24*, 3812−3815.
(35) Prosa, T. J.; Winokur, M. J.; Moulton, J.; Smith, P.; Heeger, *A. J. Macromolecules* **1992**, *25*, 4364−4372.
(36) Kawai, T.; Nakazono, M.; Yoshino, K. *J. Mater. Chem.* **1992**, *2*, 903.
(37) Kawai, T.; Nakazono, M.; Sugimoto, R.; Yoshino, K. *J. Phys. Soc. Jpn.* **1992**, *61*, 3400−3406.

DOI: 10.1021/acsmacrolett.5b00827
ACS Macro Lett. 2015, 4, 1386−1391

(38) Miller, N. C.; Cho, E.; Gysel, R.; Risko, C.; Coropceanu, V.; Miller, C. E.; Sweetnam, S.; Sellinger, A.; Heeney, M.; McCulloch, I.; et al. *Adv. Energy Mater.* **2012**, *2*, 1208−1217.
(39) Tashiro, K.; Kobayashi, M.; Kawai, T.; Yoshino, K. *Polymer* **1997**, *38*, 2867−2879.
(40) Salleo, A.; Kline, R. J.; DeLongchamp, D. M.; Chabinyc, M. L. *Adv. Mater.* **2010**, *22*, 3812−3838.
(41) Lan, Y.-K.; Huang, C.-I. *J. Phys. Chem. B* **2008**, *112*, 14857−14862.
(42) Garcia-Belmonte, G.; Vakarin, E. V.; Bisquert, J.; Badiali, J. P. *Electrochim. Acta* **2010**, *55*, 6123−6127.

DOI: 10.1021/acsmacrolett.5b00827
ACS Macro Lett. 2015, 4, 1386−1391